Proceedings of the Institute of Acoustics

THE BOUNDARY ELEMENT METHOD IN OUTDOOR NOISE PROPAGATION

S N Chandler-Wilde

Brunel University, Department of Mathematics and Statistics, Uxbridge UB8 3PH

1. INTRODUCTION

The boundary element method (BEM) is an effective method for obtaining accurate solutions to the standard Helmholtz equation governing the propagation, reflection, and scattering of monofrequency acoustic waves in a homogeneous atmosphere. The method is well-developed and has a large literature for problems of scattering by obstacles of finite size (see e.g. [17,41]), and is practicable in terms of computational resources required provided the ratio of the diameter of the scattering obstacle to the wavelength is not too large.

The first application in outdoor sound propagation appears to be the boundary element simulations of the acoustic field around standard vertical screens on a flat rigid ground surface reported by Daumas [22]. A major application to date has been to the simulation of the performance of outdoor noise barriers of arbitrary cross-section: its use in this context was introduced by Seznec [56] and is developed in [7,9,33,50]. Boundary element methods have also been proposed for investigations of effects of inhomogeneous ground cover [6,29] and for predicting noise propagation from out of cuttings [14,49].

The advantages and disadvantages of the method will become clearer in the course of the paper. To date, it is only really effective for outdoor ground surfaces which are essentially one-dimensional, meaning that there is some horizontal vector in which direction there is no change in surface elevation or in acoustical properties. Further, it is limited in practice to modelling homogeneous quiescent atmospheres, so that wind and temperature gradient effects and scattering due to atmospheric turbulence are not modelled. The method is best adapted to situations where the ground is basically flat and homogenous with only localised departures from this (e.g. strips of a different ground type, noise barriers, cuttings, etc.).

Within these limitations, since it is solving the governing wave equation to an accuracy only limited by the fineness of the discretisation of the boundary employed, it accurately models the acoustic performance of noise barriers and ground surfaces of arbitrary cross-sectional complexity and arbitrary variations in absorptive properties, and this is its great advantage over competing methods such as ray-tracing techniques [55] and parabolic equation methods [53], whose ability to treat complex diffraction and multiple scattering effects is strictly limited.

Thus, in recent years, boundary element methods have been employed to predict traffic noise propagation over inhomogeneous flat terrain [32], the performance of a range of novel noise barrier designs [18–20,34,53], the combined effects of porous asphalt surfacing and barriers on road

traffic noise [60], and the influence of the design of balconies on noise levels in tall buildings [36]. Boundary element methods have also played an important role in the validation of other, simpler but approximate methods for outdoor noise calculations [35,44,55].

In Section 2 we describe in more detail a class of outdoor noise problems that the boundary element method is suitable for, and the mathematical formulation. We also outline a method, proposed and implemented in the outdoor propagation context recently by Duhamel [25,55], by which the computationally expensive 3D problem of scattering of a spherical wave by a barrier of infinite length is reduced to a sequence of 2D problems by a partial Fourier transformation. The boundary element method is a numerical solution procedure applied to a reformulation of the Helmholtz equation as an integral equation on the boundary. In Section 3 we review the available integral equation formulations: the numerical solution procedures are discussed in Section 4. Some comparisons with experimental results are presented in Section 5, and applications of the method to outdoor noise problems, in particular to traffic noise prediction, are reviewed in Section 7. In the concluding section we briefly mention some prospects for the further development of the method, in particular the possibilities of modelling arbitrary ground surface geometries and atmospheric effects.

2. PROBLEM FORMULATION

We adopt throughout a right-handed Cartesian coordinate system $Oxyz$ with the $y-$axis vertically upwards, and restrict consideration to boundaries which are essentially one-dimensional, with no variation in geometry or in acoustical properties in the z-direction. For definiteness we suppose, at this stage, that the excitation is due to a single (monopole) point source (an incident spherical wave) or due to an infinite *coherent* line source (incident cylindrical wave case). For the line source we assume that the 'line' is parallel to the $z-$axis. We work throughout in the frequency domain, carrying out our calculations in the first instance for monofrequency sources with time dependance $e^{-i\omega t}$. Figure 1, a cross-section through the ground geometry, shows the most general situation we consider. The noise emanates from the source at S and is reflected and scattered by the boundary Γ, which includes the ground surface itself and any man-made structures, e.g. noise barriers. The boundary Γ may, as shown in the figure, have more than one component, consisting of a single infinite arc plus one or more closed curves above this, representing, for example, noise barrier elements. The connected infinite two-dimensional region above Γ we denote throughout by D.

We note at this stage that we consider the coherent line source case not because such sources are an exact model of line sources occuring in practice (e.g. road traffic streams), but because the mathematical problem becomes two-dimensional: the acoustic pressure fluctuation p depends only on the x and y coordinates of position.

Assuming a homogeneous, quiescent atmosphere (i.e. neglecting wind, temperature, and turbulence effects) the pressure p satisfies, in D, the Helmholtz equation with delta function inhomogeneity at the source position,

$$\Delta p + k^2 p = \delta_S, \tag{1}$$

where S is the source position, $\Delta = \partial^2/\partial x^2 + \partial^2/\partial y^2 + \partial^2/\partial z^2$ is the Laplacian, and $k = \omega/c$ is the wavenumber, with c the speed of sound. We restrict consideration throughout to boundaries

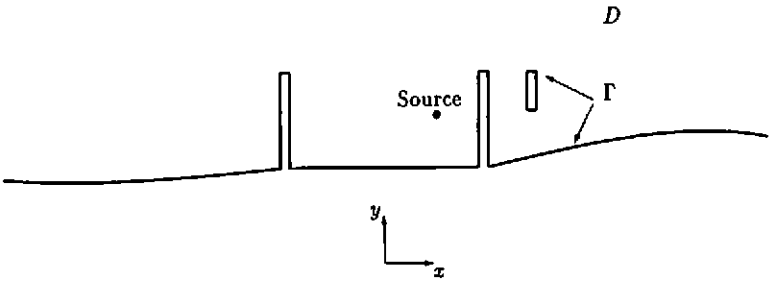

Figure 1: The geometry considered

which are locally reacting, i.e. well-modelled by the impedance boundary condition

$$\frac{\partial p}{\partial n} = ik\beta p \tag{2}$$

on Γ, where $\partial/\partial n$ denotes the derivative in the normal direction, directed out of D, and β is the boundary admittance, normalised to that of air, which is, in general, a function of both frequency and position on Γ, with $\beta = 0$ on perfectly rigid surfaces.

We do not have the space here to discuss specific expressions for β for the variety of outdoor surfaces (though see Section 6). But note that any physically appropriate impedance model satisfies that $\Re\beta \geq 0$ (to ensure the energy flow is *into* not *out of* the surface), and other constraints discussed in [37].

To complete the problem formulation we need to express mathematically the idea that the solution p we are seeking should be a wave travelling outwards from the source. In particular, we expect at least the decay associated with cylindrical or spherical spreading, i.e. that

$$r^{(n-1)/2}p \text{ remains bounded} \tag{3}$$

as $r \to \infty$, where, in the line source, two-dimensional case, $n = 2$ and r is distance from the line $x = y = 0$, while, in the point source, 3D case, $n = 3$ and r is distance form the origin. Furthermore, we impose the Sommerfeld radiation condition, that

$$r^{(n-1)/2}\left(\frac{\partial p}{\partial r} - ikp\right) \to 0 \tag{4}$$

as $r \to \infty$.

In the case when the boundary is not present, i.e. in free space, the above problem can be solved exactly. For a point source,

$$p = -\frac{e^{ikR}}{4\pi R}, \tag{5}$$

where R is the distance from the source. For a line source,

$$p = -\frac{i}{4}H_0^{(1)}(kR), \tag{6}$$

where $H_0^{(1)}$ is the Hankel function of the first kind of order zero. In the case when the boundary is present, (5) and (6) are the spherical and cylindrical waves, respectively, incident on the boundary Γ.

It was noted above that the line source/cylindrical wave is more straightforward mathematically: the problem to be solved is two-dimensional. As pointed out in the context of outdoor propagation recently by Duhamel [25,55], we can reduce the three-dimensional case of an incident spherical wave to the solution of a collection of 2D problems by representing the incident spherical wave as a linear combination of cylindrical waves. Precisely, we have that [25]

$$-\frac{e^{ikR}}{4\pi R} = -\frac{i}{8\pi}\int_{-\infty}^{+\infty} H_0^{(1)}(k_\alpha R_2)e^{i\alpha z}d\alpha, \tag{7}$$

where R is the distance from source at $(x_0, y_0, 0)$ to the receiver at (x, y, z), $k_\alpha = \sqrt{k^2 - \alpha^2}$, with $k_\alpha = i\sqrt{\alpha^2 - k^2}$ when $|\alpha| > k$, and $R_2 = ((x-x_0)^2 + (y-y_0)^2)^{1/2}$ is the distance between the source and receiver positions projected onto the plane $z = 0$. Introducing two-dimensional position vectors $\mathbf{r}_0 = (x_0, y_0)$, specifying the source position, and $\mathbf{r} = (x, y)$, specifying the first two components of the receiver position, we note that $R_2 = |\mathbf{r} - \mathbf{r}_0|$. For an incident field

$$-\frac{i}{4}H_0^{(1)}(k_\alpha R_2)e^{i\alpha z} = -\frac{i}{4}H_0^{(1)}(k_\alpha|\mathbf{r} - \mathbf{r}_0|)e^{i\alpha z}$$

we look for a reflected/scattered field in the form $P^{\text{ref}}(\mathbf{r})e^{i\alpha z}$, and this satisfies the Helmholtz equation (1) if and only if

$$P_\alpha(\mathbf{r}) = -\frac{i}{4}H_0^{(1)}(k_\alpha|\mathbf{r} - \mathbf{r}_0|) + P^{\text{ref}}(\mathbf{r}) \tag{8}$$

satisfies that

$$\Delta P_\alpha + k_\alpha^2 P_\alpha = \delta_{\mathbf{r}}, \tag{9}$$

Similarly, the impedance boundary condition (2) is satisfied if and only if

$$\frac{\partial P_\alpha}{\partial n} = ik_\alpha\beta_\alpha P_\alpha, \tag{10}$$

on Γ, where $\beta_\alpha = k_\alpha\beta/k$. Further, $P^{\text{ref}}(\mathbf{r})e^{i\alpha z}$ is an outwards travelling wave if and only if P_α satisfies (3) and (4), but with k replaced by k_α in (4), that is we require that

$$r^{1/2}P_\alpha \text{ remains bounded} \tag{11}$$

as $r \to \infty$, where r is distance from the line $x = y = 0$, and that

$$r^{1/2}\left(\frac{\partial P_\alpha}{\partial r} - ik_\alpha P_\alpha\right) \to 0 \tag{12}$$

as $r \to \infty$. We note that this method of procedure therefore reduces the problem of an incident spherical wave to the solution of equations (9)-(12), which are exactly the equations (1)-(4) to be solved in the case of an incident cylindrical wave.

Once $P_\alpha(\mathbf{r})e^{i\alpha z}$, the total field corresponding to incident field $-(i/4)H_0^{(1)}(k_\alpha|\mathbf{r}-\mathbf{r}_0|)e^{i\alpha z}$, has been computed for each α, we can calculate the pressure p at an arbitrary point (x,y,z) for a point source at $(x_0,y_0,0)$ by integrating over α, as in (7), to give that

$$p = p(x,y,z) = \frac{1}{2\pi}\int_{-\infty}^{+\infty} P_\alpha(\mathbf{r})e^{i\alpha z}d\alpha. \tag{13}$$

Frequently, we are interested in the total noise exposure due to a point source moving at uniform speed along the straight line $x = x_0$, $y = y_0$. Since, equivalently, we may move the receiver, this noise exposure (noise level due to an incoherent line source along $x = x_0$, $y = y_0$) is

$$J = \int_{-\infty}^{+\infty} |p(x,y,z)|^2 dz. \tag{14}$$

Noting that, from (13), $p(x,y,z)$ is related to $P_\alpha(\mathbf{r})$ by Fourier transformation, we have by Parseval's theorem that

$$J = \frac{1}{2\pi}\int_{-\infty}^{+\infty} |P_\alpha(\mathbf{r})|^2 d\alpha. \tag{15}$$

We usually wish to calculate noise levels associated with broad band sources, and are given source spectra which enable us to compute noise levels (SPL, L_{eq}) in each frequency band in standard conditions, e.g. in the free field. Then what is needed is to compute the *excess attenuation*, the additional attenuation due to the ground surface. For the point source or coherent line source cases this additional reduction in SPL is

$$EA = -20\log_{10}|p/p_F|, \tag{16}$$

where p_F is the pressure in free field conditions, given by (5) or (6). In the case of sources moving at uniform speed along the line $x = x_0$, $y = y_0$, (the incoherent line source case), the integral (14) is proportional to L_{eq}, and the reduction in L_{eq} due to the ground surface is

$$EA = -10\log_{10}(J/J_F), \tag{17}$$

where $J_F = 1/(16\pi R_2)$ is the value of J in the free field situation.

In practice the infinite range of integration in (13) and (15) is truncated and then the integrals are approximated by numerical integration methods which replace the integrals of (13) and (15) by finite but rather large sums (see [25,55] for proposed methods for this). Thus the problem of spherical wave scattering at a single wavenumber k is replaced with that of solving many 2D cylindrical wave scattering problems for different wavenumbers k_α. With the possibility of using this

method in mind for the point source case, we concentrate in the next three sections on the solution of the cylindrical wave scattering problem (1)-(4) (with $n = 2$), remembering that in applying these techniques to solving (9)-(12) we will wish to replace k by k_α, with $k_\alpha > 0$ for $|\alpha| < k$, but $k_\alpha = i\sqrt{\alpha^2 - k^2}$ being pure imaginary for $|\alpha| > k$.

3. BOUNDARY INTEGRAL EQUATION FORMULATIONS

A boundary integral equation (BIE) formulation for the problem consisting of equations (1)-(4) can be obtained as follows. (As indicated in the previous section, it will be enough to consider the two-dimensional case $n = 2$ of an incident cylindrical wave).

The BIE formulation depends on knowledge of exact solutions to the specified problem (1)-(4) for at least one special geometry. The simplest situation for which a solution is available is the case when the boundary is absent altogethr, i.e. the free field case, when the exact solution is given by (6). Let $\Phi(\mathbf{r}, \mathbf{r}_0)$ denote this solution, i.e.

$$\Phi(\mathbf{r}, \mathbf{r}_0) = -\frac{i}{4} H_0^{(1)}(k|\mathbf{r} - \mathbf{r}_0|), \quad \mathbf{r} \neq \mathbf{r}_0. \tag{18}$$

Then a boundary integral equation formulation can be derived as follows. Apply Green's second theorem [17] to the functions u and v, defined by $u(\mathbf{r}_s) = p(\mathbf{r}_s)$, $v(\mathbf{r}_s) = \Phi(\mathbf{r}_s, \mathbf{r})$, in the region E consisting of that part of D contained in a large circle of radius R_1 centred on the origin, excluding small circles of radius ϵ surrounding the source position $\mathbf{r}_0$, located somewhere in D, and the receiver position $\mathbf{r}$, with $\mathbf{r} \neq \mathbf{r}_0$ some point in D or on Γ. Then, since the region E excludes the singularity in u at $\mathbf{r}_0$ and in v at $\mathbf{r}$, we have that $\Delta u + k^2 u = \Delta v + k^2 v = 0$ in E so that

$$\int_{\partial E} \left(u \frac{\partial v}{\partial n} - v \frac{\partial u}{\partial n} \right) ds = 0, \tag{19}$$

where ∂E denotes the boundary of E. Letting $\epsilon \to 0$ and $R_1 \to \infty$ in (19) we obtain

$$\epsilon(\mathbf{r}) u(\mathbf{r}) = v(\mathbf{r}_0) + \int_\Gamma \left(u \frac{\partial v}{\partial n} - v \frac{\partial u}{\partial n} \right) ds \tag{20}$$

where

$$\epsilon(\mathbf{r}) = \begin{cases} 1, & \text{for } \mathbf{r} \text{ in } D, \\ \Omega(\mathbf{r})/\pi, & \text{for } \mathbf{r} \text{ on } \Gamma, \end{cases} \tag{21}$$

where $\Omega(\mathbf{r})$ denotes the interior angle in D at $\mathbf{r}$ ($= \pi$ if $\mathbf{r}$ is smooth at $\mathbf{r}$). Utilising the impedance boundary condition (2), we obtain a first BIE formulation, that

$$\epsilon(\mathbf{r}) p(\mathbf{r}) = \Phi(\mathbf{r}, \mathbf{r}_0) + \int_\Gamma \left(\frac{\partial \Phi(\mathbf{r}_s, \mathbf{r})}{\partial n(\mathbf{r}_s)} - ik\beta(\mathbf{r}_s)\Phi(\mathbf{r}_s, \mathbf{r}) \right) p(\mathbf{r}_s) ds(\mathbf{r}_s). \tag{22}$$

Equation (22), often referred to as the Helmholtz integral equation, expresses p at an arbitrary position in the region D in terms of values of p on the boundary Γ alone. Once the values of the

pressure p on the boundary Γ are known, exactly or approximately, the pressure can, in principle, be computed at any point off the boundary, by approximating the integral in (22) by a suitable numerical integration rule.

Equation (22) holds, in particular, when $\mathbf{r}$ is on Γ and, for these values of $\mathbf{r}$, is a *boundary integral equation* for the unknown pressure on the boundary Γ. This equation is solved numerically as the first stage in the *boundary integral equation method* and the values of pressure on Γ computed are used in a second stage to calculate pressure values at whichever positions are of interest off the boundary.

When we come to discuss numerical implementation in the next section we will see that it

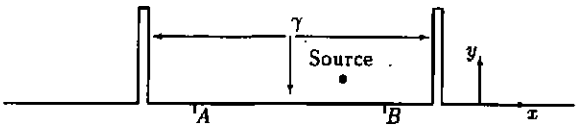

Figure 2: A local perturbation of a homogeneous plane. The surfaces are assumed to have the same constant admittance β_c, except for a localised part γ, which may consist of one or more noise barriers and part of the ground surface (AB in this case).

can be computationally very expensive to have the integral in (22) extend over the whole infinite boundary Γ. This can be avoided in cases where the ground is basically flat and uniform in surface impedance except for localised features. In particular, consider a situation such as that shown in Figure 2, where, sufficiently far away from the source, the boundary Γ coincides with the line $y = 0$. Assume also that, again sufficiently far away from the source, the boundary has a constant admittance β_c, and that any deviations from the line $y = 0$ are into the upper half-plane $y > 0$.

In the special case when the whole boundary coincides with the line $y = 0$ and has admittance β_c we have propagation above a homogeneous impedance plane and explicit expressions for the pressure can be given. Let $G_{\beta_c}(\mathbf{r}, \mathbf{r}_0)$ denote the pressure at $\mathbf{r}$ when the source is at $\mathbf{r}_0$ in this case. Then, explicitly [11],

$$G_{\beta_c}(\mathbf{r}, \mathbf{r}_0) = -\frac{i}{4} H_0^{(1)}(k|\mathbf{r} - \mathbf{r}_0|) - \frac{i}{4} H_0^{(1)}(k|\mathbf{r} - \mathbf{r}_0'|) + P_{\beta_c}(\mathbf{r}, \mathbf{r}_0), \tag{23}$$

where $\mathbf{r}_0' = (x_0, -y_0)$ is the image of the source and

$$P_{\beta_c}(\mathbf{r}, \mathbf{r}_0) = \frac{\beta_c e^{i\rho}}{\pi} \int_0^\infty t^{-1/2} e^{-\rho t} g(t)\, dt + \frac{\beta e^{i\rho(1-a_+)}}{2\sqrt{1-\beta_c^2}} \mathrm{erfc}(e^{-i\pi/4}\sqrt{\rho}\sqrt{a_+}), \quad \beta_c \neq 1, \tag{24}$$

with $\rho = k|\mathbf{r} - \mathbf{r}_0'|$, $a_+ = 1 + \beta_c \cos\theta_0 - \sqrt{1-\beta_c^2}\sin\theta_0$, $\theta_0 = \arccos((y + y_0)/|\mathbf{r} - \mathbf{r}_0'|)$ the angle of incidence, erfc the complementary error function, and

$$g(t) = -\frac{\beta_c + \cos\theta_0 (1+it)}{\sqrt{t}\sqrt{2i(t^2 - 2i(1+\beta_c\cos\theta_0)t - (\beta_c + \cos\theta_0)^2)}} - \frac{e^{-i\pi/4}\sqrt{a_+}}{2\sqrt{1-\beta_c^2}(t - ia_+)}.$$

Note that all the complex square roots in the above expressions are to be taken with non-negative real part.

Using this explicit solution we can proceed identically as in the derivation of (20), to find that (20) holds with v redefined as $v(\mathbf{r}) = G_{\beta_c}(\mathbf{r}, \mathbf{r}_0)$, provided we replace $\epsilon(\mathbf{r})$ by $\eta(\mathbf{r})$, defined by

$$\eta(\mathbf{r}) = \begin{cases} 1, & \text{if } \mathbf{r} \text{ in } D, \\ \Omega(\mathbf{r})/\pi, & \text{if } \mathbf{r} = (x, y) \text{ on } \Gamma,\ y > 0, \\ 2\Omega(\mathbf{r})/\pi, & \text{if } \mathbf{r} = (x, y) \text{ on } \Gamma,\ y = 0. \end{cases} \tag{25}$$

Utilising the impedance condition (2), and also the impedance boundary condition staisfied by G_{β_c}, we find that the integral over Γ reduces to one over γ, where γ consists of those parts of Γ on which $\beta \neq \beta_c$ or which lie above $y = 0$. Explicitly, we find that [56]

$$\eta(\mathbf{r})p(\mathbf{r}) = G_{\beta_c}(\mathbf{r}, \mathbf{r}_0) + \int_\gamma \left(\frac{\partial G_{\beta_c}(\mathbf{r}_s, \mathbf{r})}{\partial n(\mathbf{r}_s)} - ik\beta(\mathbf{r}_s) G_{\beta_c}(\mathbf{r}_s, \mathbf{r}) \right) p(\mathbf{r}_s) ds(\mathbf{r}_s), \tag{26}$$

this equation used first for numerical comuptation in Seznec [56] (but only for $\beta_c = 0$) and more recently in [7,9,33,50].

Occasionally we are interested in the case of propagation over flat ground of variable acoustic type, that is we wish to consider the case when Γ coincides with the line $y = 0$. Then, in view of the impedance condition satisfied by G_{β_c} on Γ, (26) simplifies to

$$p(\mathbf{r}) = G_{\beta_c}(\mathbf{r}, \mathbf{r}_0) + ik \int_\gamma (\beta_c - \beta(\mathbf{r}_s)) G_{\beta_c}(\mathbf{r}_s, \mathbf{r}) p(\mathbf{r}_s) ds(\mathbf{r}_s). \tag{27}$$

At this point we note that the basic Helmholtz integral equation (26) suffers from the problem

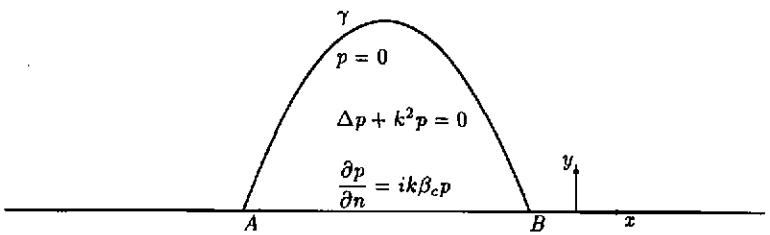

Figure 3: Case of a single mound/noise barrier and the interior problem which determines uniqueness in this case.

that there may exist wavenumbers k at which it has more than one solution, only one of which is physically correct. (The special case of equation (27) does not have this problem of non-uniqueness, as shown in [13].) Consider first the case shown in Figure 3 in which the boundary is flat, except for a single mound/noise barrier bounded above by the arc γ. In this case the integral equation has more than one solution if and only if the problem in the bounded region underneath the barrier,

shown in Figure 3, has a resonant mode. This interior problem consists of the boundary condition $p = 0$ on γ and the impedance condition $\partial p/\partial n = ik\beta_c p$ on the part of the line $y = 0$ inside the barrier. If $\Re\beta_c > 0$ (the ground is energy-absorbing) then this interior problem has no resonant modes. If the barrier is on rigid ground ($\beta_c = 0$) then this interior problem has resonant modes at an unbounded infinite sequence of positive wavenumbers, called the ***irregular wavenumbers*** for the integral equation (26). If there is more than one barrier, as in Figure 2, then there is an infinite sequence of irregular wavenumbers associated with each barrier, and if, as in Figure 1, there are components of the boundary Γ which are closed curves, disconnected from the ground surface, then there are irregular wavenumbers also associated with each of these components, these being the resonant modes for the Helmholtz equation in the component with boundary condition $p = 0$.

If k is exactly equal to one of these irregular wavenumbers then the integral equation (26) has more than one solution. There are also difficulties when numerical solution methods are employed if k is very close to an irregular wavenumber, discussed in §4.

Compared to equation (22), when computing pressures from (26) we are much better off: the integral in (26) extends only over the finite part γ of the boundary and this leads to a much reduced computation when the integral is approximated numerically. Once p is determined on the finite part of the boundary γ we can use (26) to compute p anywhere in D. We can also compute the air velocity since this is proportional to ∇p and, from (26), for $\mathbf{r}$ in D,

$$\nabla p(\mathbf{r}) = \nabla_{\mathbf{r}} G_{\beta_c}(\mathbf{r}, \mathbf{r}_0) + \int_\gamma \nabla_{\mathbf{r}} \left(\frac{\partial G_{\beta_c}(\mathbf{r}_s, \mathbf{r})}{\partial n(\mathbf{r}_s)} - ik\beta(\mathbf{r}_s) G_{\beta_c}(\mathbf{r}_s, \mathbf{r}) \right) p(\mathbf{r}_s) ds(\mathbf{r}_s). \tag{28}$$

This enables the computation also of intensity vectors.

An alternative integral equation can be obtained from (28) by taking the component of this equation in a direction normal to the boundary and then moving $\mathbf{r}$ onto the boundary, to obtain, using standard jump relations [17] and the impedance boundary condition (2) that, at points on γ with $y > 0$ which are not corner points

$$\frac{1}{2} ik\beta(\mathbf{r}) p(\mathbf{r}) = \frac{\partial G_{\beta_c}(\mathbf{r}, \mathbf{r}_0)}{\partial n(\mathbf{r})} + \int_\gamma \left(\frac{\partial^2 G_{\beta_c}(\mathbf{r}_s, \mathbf{r})}{\partial n(\mathbf{r}_s) \partial n(\mathbf{r})} - ik\beta(\mathbf{r}_s) \frac{\partial G_{\beta_c}(\mathbf{r}_s, \mathbf{r})}{\partial n(\mathbf{r})} \right) p(\mathbf{r}_s) ds(\mathbf{r}_s), \tag{29}$$

with the integral understood as a Hadamard finite part.

This second integral equation suffers from the same problem of non-uniqueness of solution if $\beta_c = 0$, though at a different set of wavenumbers. It was originally proposed by Burton and Miller [5] that an integral equation which does not have multiple solutions can be obtained by adding (26) and (29) together to obtain

$$\begin{aligned} \frac{1}{2}(1 + \kappa k\beta(\mathbf{r})) p(\mathbf{r}) = G_{\beta_c}(\mathbf{r}, \mathbf{r}_0) - i\kappa \frac{\partial G_{\beta_c}(\mathbf{r}, \mathbf{r}_0)}{\partial n(\mathbf{r})} + \int_\gamma \left(\frac{\partial G_{\beta_c}(\mathbf{r}_s, \mathbf{r})}{\partial n(\mathbf{r}_s)} - ik\beta(\mathbf{r}_s) G_{\beta_c}(\mathbf{r}_s, \mathbf{r}) \right. \\ \left. -i\kappa \left\{ \frac{\partial^2 G_{\beta_c}(\mathbf{r}_s, \mathbf{r})}{\partial n(\mathbf{r}_s) \partial n(\mathbf{r})} - ik\beta(\mathbf{r}_s) \frac{\partial G_{\beta_c}(\mathbf{r}_s, \mathbf{r})}{\partial n(\mathbf{r})} \right\} \right) p(\mathbf{r}_s) ds(\mathbf{r}_s), \end{aligned} \tag{30}$$

where κ, a positive constant, is the *coupling parameter*, the value $\kappa = 1/k$ commonly taken. This formulation has been used for the computations in Duhamel [25].

We noted previously that a requirement of the integral equation (26) is that the boundary Γ lies entirely in the upper half-plane $y \geq 0$. A frequent situation is the opposite one in which the boundary lies predominantly along the line $y = 0$ but drops occasionally into the lower half-plane $y < 0$: for example this is the case if we are modelling propagation from road traffic in a cutting onto surrounding flat ground. A modified integral equation formulation has been proposed for this case [14]. In [14] it is shown that this modified formulation has no irregular wavenumbers and in [49] a numerical treatment scheme is described and calculations of traffic noise propagation are carried out.

We have assumed in this section that all barrier elements have a finite thickness. In practice outdoor noise barriers often have a thickness small compared to the wavelength, which may be regarded as negligible. The integral equation formulation (26) does not apply in this case but modified formulations can be employed [22,40,43]. If the barrier is rigid on both sides it is computationally more efficient to employ these modified formulations and treat the barrier as having negligible thickness, as discussed in [43].

4. NUMERICAL SOLUTION METHODS

In certain special cases, good estimates of the solutions of the integral equations of Section 3 can be made [6,26,31,47,48], but usually an entirely numerical solution procedure must be employed. The *boundary element method* is invariably employed, i.e. the part of the boundary Γ over which the integration takes place is divided into small pieces (the boundary elements) and an approximation of the unknown function as a polynomial is used within each element. Usually, unless the boundary is already polygonal, say, an approximation of the boundary is also involved.

4.1 A Simple Boundary Element Method

We consider first the simplest procedure applied to the integral equation (26) by way of example. The first step is to approximate the boundary, replacing γ by a polygonal arc $\tilde{\gamma}$ composed of N straight line elements $\gamma_1, \gamma_2, \ldots, \gamma_N$. (We denote the midpoint and length of the nth element, γ_n, by $\mathbf{r}_n$ and h_n respectively, and the length of the largest element by h.) The original region D is thus replaced by a perturbed region $\tilde{D}$, and the original solution p is replaced by a perturbed solution $\tilde{p}$, unless, of course, γ is already polygonal.

The perturbed solution $\tilde{p}$ satisfies the integral equation (26), with γ, D, p replaced by $\tilde{\gamma}$, $\tilde{D}$, $\tilde{p}$. This equation can be written as (we replace D and Γ by $\tilde{D}$ and $\tilde{\Gamma}$ in the definition of η),

$$\begin{aligned}\eta(\mathbf{r})p(\mathbf{r}) &= G_{\beta_c}(\mathbf{r},\mathbf{r}_0) + \sum_{n=1}^{N}\int_{\gamma_n}\left(\frac{\partial G_{\beta_c}(\mathbf{r}_s,\mathbf{r})}{\partial n(\mathbf{r}_s)} - ik\beta(\mathbf{r}_s)G_{\beta_c}(\mathbf{r}_s,\mathbf{r})\right)p(\mathbf{r}_s)ds(\mathbf{r}_s) \\ &\approx G_{\beta_c}(\mathbf{r},\mathbf{r}_0) + \sum_{n=1}^{N}\left\{\int_{\gamma_n}\frac{\partial G_{\beta_c}(\mathbf{r}_s,\mathbf{r})}{\partial n(\mathbf{r}_s)}ds(\mathbf{r}_s) - ik\beta(\mathbf{r}_n)\int_{\gamma_n}G_{\beta_c}(\mathbf{r}_s,\mathbf{r})ds(\mathbf{r}_s)\right\}p(\mathbf{r}_n) \quad (31)\end{aligned}$$

if h (the maximum element length) is small enough so that $\tilde{p}$ and β are approximately constant on each element.

Equation (31) is satisfied approximately by $\tilde{p}$. The *exact* solution to (31) (assuming for the moment that such a solution exists) can be used to approximate $\tilde{p}$. In fact we do not solve (31) as it stands, because it is difficult to evaluate the integrals in (31) exactly. Instead we first make further approximations, replacing the integrals in (31) by approximations,

$$b(\mathbf{r},\gamma_n) \approx \int_{\gamma_n} \frac{\partial G_{\beta_c}(\mathbf{r}_s,\mathbf{r})}{\partial n(\mathbf{r}_s)} ds(\mathbf{r}_s), \tag{32}$$

$$c(\mathbf{r},\gamma_n) \approx \int_{\gamma_n} G_{\beta_c}(\mathbf{r}_s,\mathbf{r}) ds(\mathbf{r}_s), \tag{33}$$

to be discussed shortly. Thus we solve, for the approximate solution p_N, the equation

$$\eta(\mathbf{r})p_N(\mathbf{r}) = G_{\beta_c}(\mathbf{r},\mathbf{r}_0) + \sum_{n=1}^{N} \{b(\mathbf{r},\gamma_n) - ik\beta(\mathbf{r}_n)c(\mathbf{r},\gamma_n)\} p_N(\mathbf{r}_n).$$

This equation expresses p_N at an arbitrary point $\mathbf{r}$ in terms of the values of p_N at the midpoints of the N elements. To determine these N values we can set $\mathbf{r} = \mathbf{r}_n$, for $n = 1, 2, ..., N$, in (34) to obtain a system of N linear equations in the unknowns $p_N(\mathbf{r}_n)$, $n = 1, 2, ..., N$, namely

$$\sum_{n=1}^{N} a_{mn} p_N(\mathbf{r}_n) = G_{\beta_c}(\mathbf{r}_0,\mathbf{r}_m), \quad m = 1, 2, ..., N, \tag{34}$$

where

$$a_{mn} = \frac{1}{2}\delta_{mn} - b(\mathbf{r}_m,\gamma_n) + ik\beta(\mathbf{r}_n)c(\mathbf{r}_m,\gamma_n), \quad m,n = 1, 2, ..., N.$$

and $\delta_{mn} = 1$, $m = n$, $= 0$ otherwise, is the Knonecker delta. The approximations (32) and (33) are obtained by using a product midpoint rule [9], designed so as to produce errors no worse than those already introduced in (31). The approximations are specified precisely in [9].

Some comment on computational cost is appropriate. For very large N the cost of solution of the linear equations (34) dominates if a direct solution method is used ($\approx N^3/3$ multiplications are required for Gaussian elimination). For values of $N \approx 1000$ the cost of setting up the matrix $[a_{mn}]$ is important, especially if $\beta_c \neq 0$. When $\beta_c \neq 0$ this cost is dominated by the evaluation of $P_{\beta_c}(\mathbf{r}_m,\mathbf{r}_n)$ and $\partial P_{\beta_c}(\mathbf{r}_m,\mathbf{r}_n)/\partial x_s$, for $m,n = 1, ..., N$. The cost of carrying out these evaluations is halved by noting that

$$P_{\beta_c}(\mathbf{r}_m,\mathbf{r}_n) = P_{\beta_c}(\mathbf{r}_n,\mathbf{r}_m), \quad \partial P_{\beta_c}(\mathbf{r}_m,\mathbf{r}_n)/\partial x_s = -\partial P_{\beta_c}(\mathbf{r}_n,\mathbf{r}_m)/\partial x_s.$$

Once the values of p_N at the element midpoints have been obtained by solving (34), the subsequent calculation of p_N at an arbitrary point $\mathbf{r}$ in D using (34) has a very much smaller computational cost, proportional to N.

Regarding the size of N required, it is found that the maximum element length h must not exceed $\lambda/5$, where λ is the wavelength, and element lengths smaller than this are desirable. Thus, the ratio $|\gamma|/\lambda$, where $|\gamma|$ is the length of γ, the part of the boundary discretised, plays a crucial role in determining the cost of computations.

4.2 Accuracy of this Scheme

Provided the wavenumber is not such that the integral equation (26) has more than one solution – see §3 – the above approximation p_N will exist (i.e. (34) will have a solution) and will converge to the true solution p as $h \to 0$. In the case of a polygonal barrier this convergence can be shown using ideas of Bruhn and Wendland [4]. For the particular case of the integral equation (27), which we recall does not have any irregular wavenumbers, even if $\beta_c = 0$, the convergence of essentially this numerical scheme has been established in Ross [54]: moreover the maximum error in the predicted values of pressure on the boundary is shown to be

$$\leq C_\epsilon kh(1 + |\log(kh)|),$$

provided $\Re\beta \geq \epsilon$, $|\beta| \leq 1/\epsilon$, where the constant C_ϵ depends on ϵ and on β_c but not on k or the length of the interval of integration γ. (This appears to be the first error estimate for the boundary element method in acoustic scattering in which the dependence of the error on k is made explicit.) In [8] the dependence of the error on h for equation (27) is investigated further in the case $\beta_c = 0$, and it is shown that, for a fixed piecewise constant admittance variation and fixed wavenumber k, the error is $O(h^{2-\epsilon})$ for every $\epsilon > 0$. (That is the convergence rate is almost proportional to h^2 which is the best that can possibly be achieved in general when solving (26) or (27) using a piecewise constant approximation.)

However, if there exist wavenumbers k^* at which the integral equation has more than one solution, which there must if $\beta_c = 0$ and part of the boundary lies above $y = 0$, then the accuracy must deteriorate near these wavenumbers. Amini and Kirkup [2] investigate this behaviour theoretically and experimentally for the method of §4.1 applied to scattering by a rigid circular obstacle and find that, very near k^*, the error $\approx Ch^2/|k - k^*|$, where C is a constant. In their experiments, when the wavenumber k is within 0.06% of the value of k^* the accuracy deteriorates by a factor of approximately 70. Although these deteriorations in accuracy are modest, because the position of the irregular wavenumbers k^* is *a priori* unknown for general scattering shapes, so that $|k - k^*|$ is unknown, they recommend adoption of the Burton and Miller formulation [5], (30) in our context, and this has been adopted in recent computations by Duhamel [25].

4.3 More Sophisticated Boundary Element Methods

Accuracy can be improved by using higher degree polynomials to approximate the solution: but improvements in accuracy can be fairly modest if discontinuities in admittance are present or, worse, re-entrant corners (corners on Γ with interior angle $\Omega(\mathbf{r}) > \pi$). At such points the velocity and thus ∇p is predicted by the Helmholtz equation to be infinite. This is an undesirable inadequacy of the Helmholtz equation as a model of noise propagation, but also it has unfortunate consequences for the accuracy of numeriacl; schemes if carried out in a naive way, since polynomials are not ideally

suited to representing functions with such singularities. In [8] results are reported of solving (27) using both piecewise constant and piecewise quadratic approximations on a uniform grid, for a case (as is usual in practice) when β is piecewise constant. The results for the piecewise quadratic case are approximately 6 times more accurate for the same number of degrees of freedom N, but there is no improvement, either observed or theoretically predicted, in the rate of convergence as $h \to 0$. Faster rates of convergence *can* be obtained by using higher degree polynomials when admittance discontinuities and/or re-entrant corners are present but only by either representing the singularities in the solution explicitly so that only a smoother remainder is approximated by polynomials, as in [8] for equation (27), or by the use of graded meshes, i.e. by using smaller and smaller element sizes as the admittance discontinuity/corner is approached, but in such a way that the total number of elements is not increased significantly. The application of such methods to boundary integral equations is reviwed in [3], and see [24] where both mesh grading and variable degrees of polynomial approximation are employed to obtain very rapid convergence rates for obstacle scattering problems.

When using higher degree polynomials to approximate the unknown pressure on the boundary it is usual at the same time to use the same degree of polynomial approximation to represent the boundary shape, via the use of so-called *isoparametric elements* [15]. In Park and Eversman [50] the use of cubic isoparametric elements to solve (26) is reported, while in Duhamel [25] quadratic elements are employed in the solution of (30).

We remark finally that accuracy of the numerical solution can be assessed: this is done most simply by running an extra simulation with double the number of elements, to assess the accuracy of the original predictions. This can be an expensive procedure however. An alternative error estimate (though not clearly superior) is described in the context of scattering by obstacles in [27]. Reference [] also recommends the Galerkin BEM for setting up the linear system (34), rather than the collocation method employed in Section 4.1 and in [25,50]. (More precisely, the method of Section 4.1 is an iterated collocation method which usually has improved accuracy.) For an explanation of these terms and a discussion of the attractive mathematical properties of the Galerkin method see [3].

4.4 Computation of $P_{\beta_c}(\mathbf{r}, \mathbf{r_0})$

The first two terms in a uniformly valid asymptotic expansion of $P_{\beta_c}(\mathbf{r}, \mathbf{r_0})$ in the far field ($\rho = k|\mathbf{r} - \mathbf{r_0'}|$ large) are given in [6], and this approximation for P_{β_c} is used for the boundary element calculations in [43]. The full far field asymptotic expansion, and a proof of its uniform validity, are obtained in [12] but, for numerical computations, the authors recommend numerical integration of the representation (24), derived in [11], if β_c is not too close to 1. It is proved in [11] that the representation (24) can be accurately evaluated by Gauss quadrature with weight function $t^{-1/2}e^{-\rho t}$ and explicit error estimates are given which show that this procedure is extremely accurate in the far field. Numerical calculations show that, using only a 22 point rule, an approximation is generated which is very accurate except in the very near field. An alternative representation for P_{β_c} when β_c is close to 1 is also derived, and similar representations for $\partial P_{\beta_c}(\mathbf{r}, \mathbf{r_0})/\partial x$ are obtained. It is

shown that

$$\frac{\partial P_{\beta_c}(\mathbf{r}, \mathbf{r}_0)}{\partial y} = -2ik\beta_c \Phi(\mathbf{r}, \mathbf{r}_0') - ik\beta_c P_{\beta_c}(\mathbf{r}, \mathbf{r}_0), \tag{35}$$

and it is pointed out in [10], or see [43], that higher partial derivatives of P_{β_c}, such as are needed in (30), can be computed from P_{β_c} and $\partial P_{\beta_c}/\partial x$ using (35) and the Helmholtz equation,

$$(\Delta + k^2) P_{\beta_c}(\mathbf{r}, \mathbf{r}_0) = 0$$

satisfied by P_{β_c}.

5. COMPARISONS WITH EXPERIMENTAL RESULTS

We show in this section some results illustrating the use of the BEM of §4.1 and comparing numerical and scale model experimental results.

In the graphs shown below predicted and experimentally measured values of excess attenuation (given by (16)) or of insertion loss (reduction in dB level on inserting the noise barrier) are plotted. For each of the experiments a point source of sound is used and the receiver position is in the same plane perpendicular to the noise barrier as the source. The numerical results are obtained by replacing the point source of sound by a coherent line source, the line source passing through the position of the point source parallel to the noise barrier.

For the results shown in Figures 4 and 5 elements of size $\lambda/5$ were used at each frequency. For the results in Figure 6 this size element was used at the higher frequencies but a smaller element size (as a fraction of the wavelength but not in absolute terms) was used at lower frequencies.

Figures 4 and 5(b) show comparisons between the numerical model and experimental results for barriers on absorbing ground. For the numerical results the admittance β_c of the absorbing ground is calculated using the Delany and Bazley formulae [23] which give the relative admittance (β_G) and complex wavenumber (k_G) of a porous medium as functions of σ/f, where σ is an effective flow resistivity and f is the frequency. Modelling the ground as a porous layer of thickness T on top of a rigid half-space, and assuming that the ground is locally reacting, the surface admittance β_c is given by

$$\beta_c = \beta_G \tanh(-iTk_G). \tag{36}$$

Figure 4 shows the results of an outdoor model experiment on grassland carried out by Rasmussen [52] for the geometry indicated using a three-sided barrier. The ground is modelled as a porous half-space ($T = +\infty$ in (36)) and the flow resistivity σ is calculated so as to give the best fit between experimental measurements of EA and theoretical values in the absence of the barrier. The agreement between 1/3-octave band experimental measurements and numerical model results is good.

Figure 5 compares experimental measurements in an anechoic chamber at Bradford University,

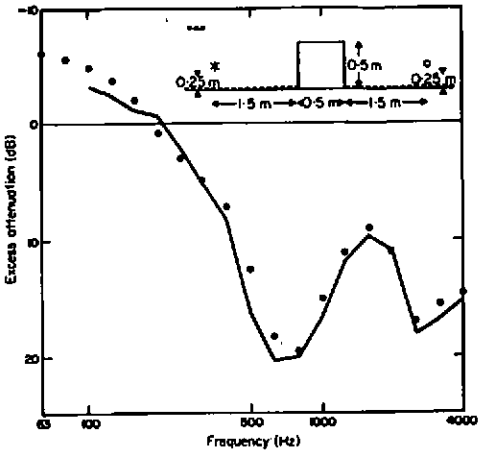

Figure 4: Comparison of third-octave band measurements (——) [52] with BEM predictions (•) calculated at third-octave centre frequencies. The barrier surface is rigid and the ground has effective flow resistivity $\sigma = 250000\text{Nsm}^{-4}$.

reported in [7], with theoretical predictions. In this case the barrier is semi-circular, with a hard plastic surface, and sits on a flat formica-covered chipboard surface, modelling an infinite rigid plane. In Figure 5(b) both the barrier and the ground plane are made absorbing by covering them with an 8mm thick carpet (thus $T = 8$mm in equation (36)). A value $\sigma = 500000\text{Nsm}^{-4}$ is selected for use in equation (36), again by fitting to propagation measurements above a homogeneous plane. The agreement between experiment and theory for the rigid surface case is excellent in Figure 5(a): also shown is a Fourier-Bessel series analytical solution to the problem of diffraction of a cylindrical wave by a semi-circular barrier on a rigid plane, given in [50]. The agreement is good over most of the frequency range also in the case of absorbent surfaces (Fig 5(b)). The differences which do occur may be due to an inadequacy of the Delany-Bazley model as a description of the surface admittance of the carpet.

The final two graphs (Figure 6) show comparisons of BEM predictions and experimental measurements in the same anechoic chamber, taken from [9]. The measurements are at a scale of 1:20: the graphs plot frequency values and show length dimensions in metres at full scale: the actual measured frequency values are 20 times higher. In both graphs the experimental measurements are over 2.5Hz bands (at full scale): the experimental average is formed by taking a mean dB value for each group of 10 adjacent bands. Theoretical values are calculated at the frequencies 25,50,...,1000 Hz.

In the two graphs in Figure 4 agreement between BEM and measured values is generally good. The scatter in both the experimental and theoretical values in Figure 4(b) may be due to reflections between the two vertical barriers. Futher boundary element predictions for such multiple noise barrier configurations are contained in [19], and for further comparisons of the BEM with

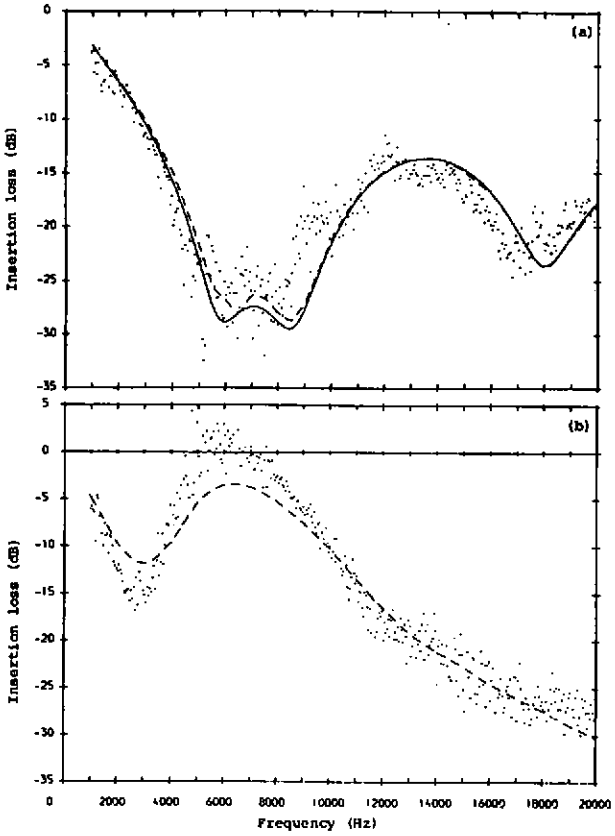

Figure 5: Insertion loss for a semi-circular barrier on a homogeneous plane. (·) experimental; (— —) analytical; (- - - -) BEM. The source and receiver coordinates are $x_0 = 0.5$m, $y_0 = 0.048$m, $x = 0.5$m ((0,0) is the centre of the barrier). (a) $y = 0.0465$m, rigid barrier and plane; (b) $y = 0.046$m, carpeted barrier and plane.

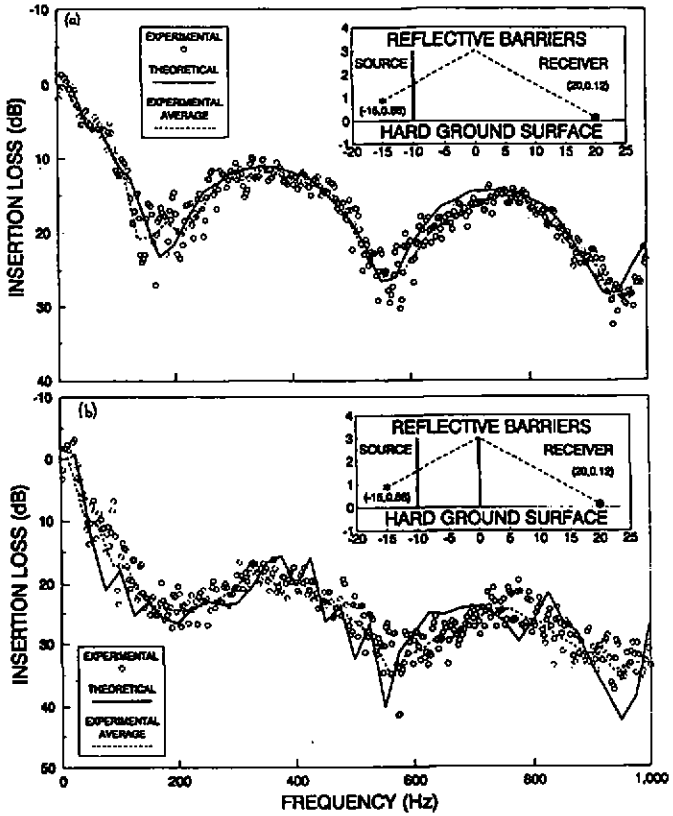

Figure 6: Comparisons of experimental scale model measurements (scale 1:20) with BEM predictions for a single 3m barrier (a) and two parallel 3m barriers (b). The fullscale geometry is as indicated with dimensions in metres.

measurements see [20,50,57].

6. OUTDOOR NOISE CONTROL PREDICTIONS

We review briefly here the ways in which the BEM has been used to make predictions of the performance of noise control elements outdoors. Predominantly, for efficiency (so as to obtain a two-dimensional problem), in these predictions the sound source has been represented as one or more coherent line sources, rather than using the computationally more expensive method recently implemented by Duhamel [25] and discussed in §2 which accurately predicts propagation from a point or incoherent line source. As demonstrated and discussed already in §5, comparisons with scale model experimental measurements for single noise barriers on flat ground show that computations with a coherent line source can be used to accurately predict excess attenuation or insertion loss for a point source of sound, provided that the receiver is in the same plane perpendicular to the noise barrier as the source. This conclusion is backed up by comparisons with full scale outdoor measurements of insertion loss spectra for single and multiple noise barriers under close to zero wind conditions [57,Figure 13] and by comparisons of point source and coherent line source BEM predictions of excess attenuation for various shapes of single barriers [25].

However, predominantly, noise barriers are used to screen road traffic streams and rail noise, which are more appropriately modelled, for the purpose of calculating L_{eq} values, by incoherent line sources. In general, insertion loss values are lower for an incoherent line source than for a point source at normal incidence (see, for example, the calculations in [39] or [25]). Thus insertion loss values computed with a coherent line source cannot be used directly e.g. for predicting road traffic noise L_{eq} values. (The same observation applies to scale model and outdoor measurements carried out with point sources [38,46].) However, there is some evidence from the scale model tests of Koyasuta and Yamashita [42], that, as far as the relative screening performances of different barrier configurations for broad band spectra are concerned, predictions for a point source at normal incidence (and thus for a coherent line source) agree well with measurements for an incoherent line source.

In a series of papers, extensive computations, using the BEM described in §4.1, of the acoustic performance of a range of noise barrier designs have been carried out using a coherent line source (approximating a point source at normal incidence, as indicated above). For the reasons already discussed, the predictions of relative insertion loss made are likely to be of most value, and for the most part predictions are presented in the literature of the performance of more complicated noise barrier-designs relative to the performance of a standard thin vertical barrier of the same or some reference height. This is the procedure also followed in the scale model experimental studies of [38,46] and makes sense also in the respect that absolute insertion loss values depend strongly on source and receiver positions and on ground type.

A range of cross-sectional shapes, and the effects on them of absorptive coverings, are examined in Hothersall et al. [33]. In particular the insertion losses of standard vertical screens, T-profile and semi-circular barriers, and of wedge shaped barriers of different wedge angles are compared. The performance of T-profile and related shape barriers is considered in more detail in [34] and

the performance of several parallel screens between a road traffic source and a receiver is explored in [19]. Also in [19], and in more detail in [20], the performance of multiple-edged barriers with a single foundation is investigated. Typical results from these investigations are shown in Figure 7, reproduced from [20]. The results shown are, for design (a), the mean insertion loss over six receiver positions, located at heights of 1.5m and 3m, distances 20, 50, and 100m from the barrier centre line, on the opposite side to the source, which is 15m from the centre line in the rigid ground surface, and has a broad band spectrum representative of A-weighted road traffic noise [33]. For the other designs the figures are ΔIL, the mean improvement in insertion loss over the same six positions, relative to a standard reflective vertical barrier (design (a)).

The boundary element simulations shown in Figure 7, and others in [19,20], led to full-scale tests at a purpose-built noise barrier test facility at the Transport Research Laboratory and to comparisons of BEM predictions with these experiments [57], and later to the testing of multiple-edged designs on the M25 [59]. Further full-scale tests and boundary element simulations of the performance of a complex commercial design are reported in [58]. Recently, using the approximate boundary element procedure described in [47], predictions of the acoustical effectiveness of porous asphalt (PA) in place of hot-rolled asphalt (HRA) have been obtained [60], and the effect of barriers on one or both sides of a motorway on the advantage of PA over HRA has been investigated. Computations, using the same BEM of §4.1, of the screening of road traffic noise by balconies on tall buildings, and the effect of absorptive treatment of these balconies are reported in [36].

7. CONCLUSIONS

We hope that it has been made clear in the course of the paper that the boundary element method is an effective method for predicting accurately effects on noise levels of a variety of outdoor features, including effects due to one or several barriers of arbitrary cross-section and surface treatment, effects of other localised variations in ground cross-section, the influence of ground type and variations in ground type, and interactions between these effects.

The boundary element methods which have been described have the limitation that atmospheric effects are not taken into account, and comparisons with measurements discussed in Section 6 have been with indoor scale model experiments or with outdoor measurements at low wind speed.

In principle, the methods can be extended to predict effects of simple wind gradient profiles, and boundary element results for a linear with height sound speed profile, showing scattering from a bump or trough in the ground surface, are reported in [45]. The Helmholtz integral equation (22) is employed, with Φ replaced by the free-field Green's function for a linear sound speed profile. The practical difficulty is that this Green's function is much more costly to compute and that, even in the homogeneous case, the integral equation (22), in which the integration is over the whole boundary Γ, is expensive to compute with. As a consequence it is not, perhaps, surprising that the results in [45] are limited to short ranges (up to 20m) at low frequency (100 Hz): i.e. computations are carried out only to a distance of ≈ 7 wavelengths from the source.

In a similar vein, the restriction in this paper to one-dimensional boundary geometries is a question

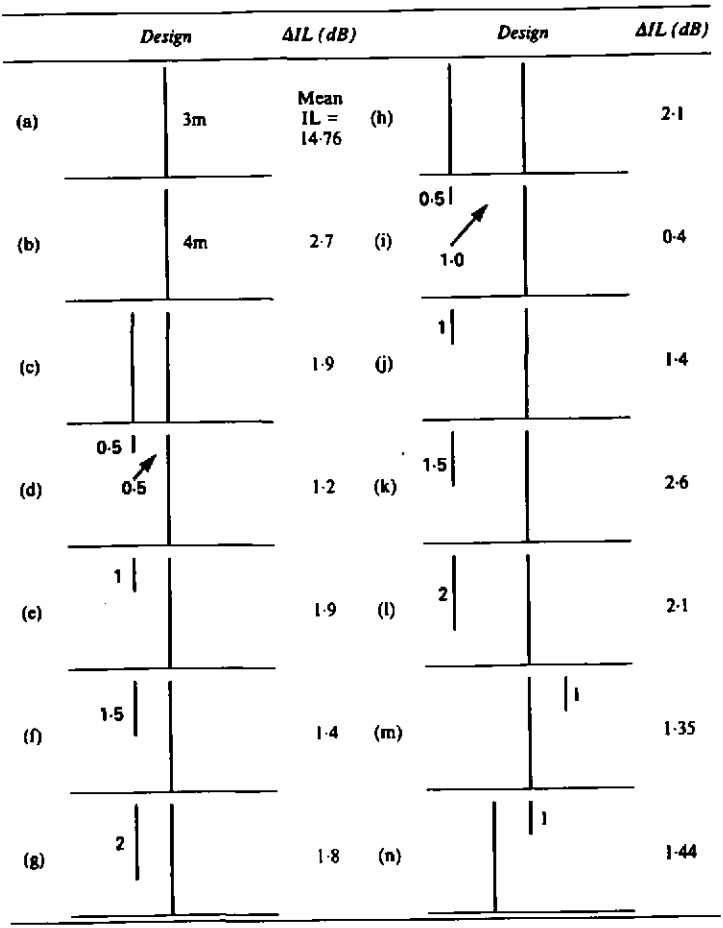

Figure 7: Comparison of different multiple-edge barrier designs. The height of all designs is 3m, the thickness of the main screen is 0.2m, and all other surfaces have a thickness of 0.1m. All dimensions are in m and those not given can be deduced from designs (e) and (k). Absorbing treatment of the barrier is indicated (- - -) and corresponds to a surface impedance given by $\sigma = 20000\text{Nsm}^{-4}$, T =0.1m in (36).

of cost rather than one of principle. Boundary element predictions for more general geometries, in particular finite length barriers, are reported for example in [40], and are used in [44] to justify a simple method for accurate prediction of finite barrier insertion loss. But, again, these predictions have been limited to low frequencies and/or small barrier sizes. A comparison of the costs of computation of spherical wave scattering by reduction to a sequence of cylindrical wave scattering problems, as described in Section 2, and by a direct 3D simulation, is given in Duhamel [25], where the 3D simulation is shown to be orders of magnitude more expensive.

As the above remarks indicate, the full power of the boundary element method is currently limited by considerations of computational cost (both CPU times and RAM required for the large full matrices generated). Future increases in computing power will improve the situation (and see [28] for a recent implementation for an acoustic scattering problem on a parallel processor). But there are also very significant algorithmic developments underway in the boundary element treatment of wave scattering problems which space does not permit me to mention in detail. Briefly, there are prospects for bringing down both the main costs of the method – construction of the full matrix in (34) and the subsequent solution of the linear system – by iterative solution techniques (multigrid and Krylov subspace methods [3], and other methods for the construction of approximate matrix inverses [1]) and by compression techniques which avoid explicit construction of the full matrix (panel clustering [30], multipole methods [16], wavelet methods [21]). For the particular integral equation (27), in the first instance, research is currently underway at Brunel [51], using some of these techniques, to reduce the computation time from one proportional to N^2 or N^3, where N is the number of boundary elements, to one proportional to $N \log N$.

Undoubtedly, there is ample scope for the development, by mathematicians and engineers, of more sophisticated and powerful boundary element methods for outdoor noise problems, and for their use as a tool in the further refinement of outdoor noise control measures.

8. ACKNOWLEDGEMENTS

The work reviewed above owes much to my many collaborators and research students. I mention in particular Donald Crombie, Philip Morgan, Andrew Peplow, Mizanur Rahman, and Chris Ross, and my collaborators Kirill Horoshenkov and David Hothersall at the University of Bradford and Greg Watts at the Transport Research Laboratory. This work is supported by a research grant from the Engineering and Physical Sciences Research Council.

9. REFERENCES

[1] S AMINI, 'An iterative method for the boundary element solution of the exterior acoustic problem', *J. Comp. Appl. Math.*, 20 p.109 (1987)

[2] S AMINI & S M KIRKUP, 'Solution of Helmholtz equation in the exterior domain by elementary boundary integral methods', *J. Comp. Phys.*, 118 p.208 (1995)

[3] K E ATKINSON, 'The Numerical Solution of Integral Equations of the Second Kind', CUP (1997).

[4] G BRUHN & W WENDLAND, 'Über die näherungsweise Lösung von linearen Funktionalgleichungen', in *Functionalanalysis, Approximations-theorie, Numerische Mathematik*, Birkhäuser

(1967)
[5] A J BURTON & G F MILLER, 'The application of integral equation methods to the numerical solution of some exterior boundary value problems', *Proc. R. Soc. Lond. A*, 323 p. 201 (1971)
[6] S N CHANDLER-WILDE & D C HOTHERSALL, 'Sound propagation above an inhomogeneous impedance plane', *J. Sound Vib.*, 98 p.475 (1985)
[7] S N CHANDLER-WILDE& D C HOTHERSALL, 'The boundary integral equation method in outdoor sound propagation', *Proc. Inst. Acoust.*, 9 p.37 (1987)
[8] S N CHANDLER-WILDE & M J C GOVER 'On the application of a generalization of Toeplitz matrices to the numerical solution of integral equations with weakly singular convolution kernels', *IMA J. Num. Anal.*, 9 p.525 (1989)
[9] S N CHANDLER-WILDE, D C HOTHERSALL, D H CROMBIE, & A T PEPLOW, 'Efficiency of an acoustic screen in the presence of an absorbing boundary'. in *Ondes Acoustiques et Vibratoires, Interaction Fluide-Structures Vibrantes*, Publ. du CNRS Lab. de Mécanique et d'Acoustique No. 126, p.73 (1991)
[10] S N CHANDLER-WILDE& D C HOTHERSALL,'On the Green's Function for Two-Dimensional Acoustic Propagation Above a Homogeneous Impedance Plane', Res. Rept., Dept Civ. Eng., Univ. Bradford. (1991)
[11] S N CHANDLER-WILDE& D C HOTHERSALL, 'Efficient calculation of the Green's function for acoustic propagation above a homogeneous impedance plane', *J. Sound Vib.*, 180 p.705 (1995)
[12] S N CHANDLER-WILDE& D C HOTHERSALL, 'A uniformly valid far field asymptotic expansion for the Green's function for two-dimensional propagation above a homogeneous plane' *J. Sound Vib.*, 182 p.665 (1995)
[13] S N CHANDLER-WILDE, 'The impedance boundary value problem for the Helmholtz equation in a half-plane', *Math. Meth. Appl. Sci.*, 20 p.813 (1997)
[14] S N CHANDLER-WILDE& A T PEPLOW, 'A boundary integral equation formulation for the Helmholtz equation in a locally perturbed half-plane', submitted to *J. Integral Eq. Appl.*
[15] G CHEN & J ZHOU, 'Boundary element methods', Academic Press (1992)
[16] J M SONG, C C LU, & W C CHEW, 'Multilevel fast multipole algorithm for electromagnetic scattering by large complex objects', *IEEE Trans. Ant. Prop.*, 45 p.1488 (1997)
[17] D COLTON & R KRESS, 'Integral equation methods in scattering theory', Wiley (1993)
[18] D H CROMBIE, 'Novel designs for road traffic noise barriers', PhD Thesis, Univ Bradford (1993)
[19] D H CROMBIE& D C HOTHERSALL, 'The performance of multiple noise barriers', *J. Sound Vib.*, 176 p.459 (1994)
[20] D H CROMBIE, D C HOTHERSALL, & S N CHANDLER-WILDE, 'Multiple-edged noise barriers', *Appl. Acoust.*, 44 p.353 (1995)
[21] W DAHMEN, S PRÖSSDORF, & R SCHNEIDER, 'Wavelet approximation methods for pseudodifferential equations II: matrix compression and fast solution', *Adv. Comp. Math.*, 1 p.259 (1993)
[22] A DAUMAS, 'Etude de la diffraction par un écran mince disposé sur le sol', *Acustica*, 40 p.213 (1978)
[23] M E DELANY & E N BAZLEY, 'Acoustic properties of fibrous absorbent materials', *Appl. Acoust.*, 3 p. 105 (1970)

[24] L DEMKOWICZ, J T ODEN, M AINSWORTH, & P GENG, 'Solution of elastic scattering problems in linear acoustics using $h-p$ boundary element methods', *J. Comput. Appl. Math.*, 36 p.29 (1991)
[25] D DUHAMEL, 'Efficient calculation of the 3-dimensional sound pressure field around a noise barrier', *J. Sound Vib.*, 197 p.547 (1996)
[26] J DURNIN & H L BERTONI, 'Acoustic propagation over ground having imhomogeneous surface impedance', em J. Acoust. Soc. Am., 70 p.852 (1981)
[27] P GENG, J T ODEN, & L DEMKOWICZ, 'Numerical solution and a posteriori error estimation of exterior acoustics problems by a boundary element method at high wave numbers', *J. Acoust. Soc. Am.*, 100 p.335 (1996).
[28] P GENG, J T ODEN, & R A VAN DE GEIJN, 'Massively parallel computation for acoustical scattering problems using boundary element methods', *J. Sound Vib.*, 191 p.145 (1996)
[29] D HABAULT, 'Sound propagation above an inhomogeneous impedance plane: boundary integral equation methods', *J. Sound Vib.*, 100 p. 55 (1985)
[30] W HACKBUSCH & Z NOWAK, 'On the fast matrix multiplication in the boundary element method by panel clustering', *Numer. Math.*, 54 p.463 (1989)
[31] J N B HARRIOTT, S N CHANDLER-WILDE& D C HOTHERSALL, 'Long distance sound propagation over an impedance discontinuity', *J. Sound Vib.*, 148 p.365 (1991)
[32] D C HOTHERSALL& S N CHANDLER-WILDE, 'Prediction of the attenuation of road traffic noise with distance', *J. Sound Vib.*, 115 p.459 (1987)
[33] D C HOTHERSALL, S N CHANDLER-WILDE, & N M HAJMIRZAE, 'Efficiency of single noise barriers', *J. Sound Vib.*, 146 p.303-322. (1991)
[34] D C HOTHERSALL, D H CROMBIE, & S N CHANDLER-WILDE, 'The performance of T-profile and associated noise barriers', *Appl. Acoust.*, 32 p.269 (1991)
[35] D C HOTHERSALL& J N B HARRIOTT, 'Approximate models for sound propagation above multi-impedance plane boundaries', *J. Acoust. Soc. Am.*, 97 p.918 (1995)
[36] D C HOTHERSALL, K V HOROSHENKOV, & S E MERCY, 'Numerical modelling of the sound field near a tall building with balconies near a road', *J. Sound Vib.*, 198 p.507 (1996)
[37] K V HOROSHENKOV, S N CHANDLER-WILDE, & D C HOTHERSALL, 'On the behaviour of some existing models for the acoustic properties of rigid frame porous media', submitted to *J. Acoust. Soc. Amer.*
[38] D A HUTCHINS, H W JONES, & L T RUSSELL, 'Model studies of barrier performance in the presence of ground surfaces. Part II-different shapes.', *J. Acoust. Soc. Am.*, 75 p. 1817 (1984)
[39] I ISEI, T F W EMBLETON, & J E PIERCEY, 'Noise reduction by barriers on finite impedance ground', *J. Acoust. Soc. Am.*, 67 p.46 (1980)
[40] Y KAWAI & T TERAI, 'The application of integral-equation methods to the calculation of sound attenuation by barriers', *Appl. Acoust.*, 31 p.101 (1990)
[41] R E KLEINMAN & G F ROACH. 'Boundary integral equations for the three-dimensional Helmholtz equation', *SIAM Rev.*, 16 p.214 (1974)
[42] M KOYASUTA & M YAMASHITA. 'Scale model experiments on noise reduction by acoustic barrier of a straight line source', *Appl. Acoust.*, 3 p.233 (1973)
[43] L A DeLACERDA, L C WROBEL, & W J MANSUR, 'A dual boundary element formulation for sound propagation around barriers over an impedance plane', *J. Sound Vib.*, 202 p.235 (1997)

[44] Y W LAM & S C ROBERTS, 'A simple method for accurate prediction of finite barrier insertion loss', *J. Acoust. Soc. Am.*, 93 p.1445 (1993)
[45] Y L LI, S J FRANKE, & CH LIU, 'Wave scattering from a ground with a Gaussian bump or trough in an inhomogeneous medium', *J. Acoust. Soc. Am.*, 94 p.1067 (1993)
[46] D N MAY & M M OSMAN, 'Highway noise barriers: new shapes', *J. Sound Vib.*, 71, p.73 (1980)
[47] P A MORGAN, C R ROSS, & S N CHANDLER-WILDE, 'An efficient boundary element model for the performance of parallel noise barriers', *Proc. Inst. Acoust.*, 17 p.465 (1995)
[48] P A MORGAN, C R ROSS, & S N CHANDLER-WILDE, 'An efficient boundary element method for noise propagation from cuttings', *Proc. INTERNOISE*,Book 6, p.3011 (1996)
[49] A T PEPLOW & S N CHANDLER-WILDE, 'Noise propagation from a cutting of arbitrary cross-section and impedance', submitted to *J. Sound Vib.*
[50] J M PARK & W EVERSMAN, 'A boundary element method for propagation over absorbing boundaries', *J. Sound Vib.*, 175 p.197 (1994)
[51] M RAHMAN, 'Numerical treatment of a class of second kind integral equations on the real line', MSc Dissertation, Brunel Univ. (1996)
[52] K B RASMUSSEN, 'Sound propagation over non-flat terrain', Danish Acoust. Lab. Rep. No. 35 (1982)
[53] J S ROBERTSON, W L SIEGMANN, & M J JACOBSON, 'Low frequency sound-propagation modeling over a locally reacting boundary with the parabolic approximation', *J. Acoust. Soc. Amer.*, 98 p.1130 (1995)
[54] C R ROSS, 'Direct and inverse scattering by rough surfaces', PhD Thes., Brunel Univ. (1997)
[55] E M SALOMONS, A C GEERLINGS, & D DUHAMEL, 'Comparison of a ray model and a Fourier-boundary element method for traffic noise situations with multiple diffractions and reflections', *Acustica*, 83 p.35 (1997)
[56] R SEZNEC, 'Diffraction of sound around barriers: use of the boundary elements technique', *J. Sound Vib.*, 73 p.195 (1980)
[57] G R WATTS, D H CROMBIE, & D C HOTHERSALL, 'Acoustic performance of new designs of traffic noise barriers: full scale tests', *J. Sound Vib.*, 177 p.289 (1994).
[58] G R WATTS & P A MORGAN, 'Acoustic performance of an interference type noise barrier profile', *Appl. Acoust.*, 49 p.1 (1996)
[59] G R WATTS, 'Acoustic performance of a multiple edge noise barrier profile at motorway sites', *Appl. Acoust.*, 47 p.47 (1996)
[60] G R WATTS, S N CHANDLER-WILDE, & P A MORGAN, 'The combined effects of porous asphalt surfacing and barriers on traffic noise', submitted to *Appl. Acoust.*